

Defect Physics of Pseudo-cubic Mixed Halide Lead Perovskites from First Principles

Arun Mannodi-Kanakithodi,^{1, a)} Ji-Sang Park,² Alex B. F. Martinson,³ and Maria K.Y. Chan^{1, b)}

¹⁾*Center for Nanoscale Materials, Argonne National Laboratory, Argonne, Illinois 60439, USA*

²⁾*Department of Materials, Imperial College London, London SW7 2AZ, United Kingdom*

³⁾*Materials Science Division, Argonne National Laboratory, Argonne, IL 60439, USA*

(Dated: 16 August 2019)

Owing to the increasing popularity of lead-based hybrid perovskites for photovoltaic (PV) applications, it is crucial to understand their defect physics and its influence on their optoelectronic properties. In this work, we simulate various point defects in pseudo-cubic structures of mixed iodide-bromide and bromide-chloride methylammonium lead perovskites with the general formula $\text{MAPbI}_{3-y}\text{Br}_y$ or $\text{MAPbBr}_{3-y}\text{Cl}_y$ (where y is between 0 and 3), and use first principles based density functional theory computations to study their relative formation energies and charge transition levels. We identify vacancy defects and Pb on MA anti-site defect as the lowest energy native defects in each perovskite. We observe that while the low energy defects in all $\text{MAPbI}_{3-y}\text{Br}_y$ systems only create shallow transition levels, the Br or Cl vacancy defects in the Cl-containing perovskites have low energy and form deep levels which become deeper for higher Cl content. Further, we study extrinsic substitution by different elements at the Pb site in MAPbBr_3 , MAPbCl_3 and the 50-50 mixed halide perovskite, $\text{MAPbBr}_{1.5}\text{Cl}_{1.5}$, and identify some transition metals that create lower energy defects than the dominant intrinsic defects and also create mid-gap charge transition levels.

The likelihood of defect formation and the positioning of defect levels with respect to band edges are both critically important for applications that are concerned with a semiconductor's optoelectronic characteristics¹⁻⁷. Native point defects could arise as a means of compensation for the presence of impurities, and lead to unintentional conductivity or counteract the prevailing conductivity. Diffusion of impurity atoms in a semiconductor—something that typically happens interstitially—could be assisted by the presence of vacancy defects. Further, “deep” electronic levels created by low energy defects in the semiconductor band gap adversely affect photovoltaic (PV) performance by potentially causing nonradiative recombination of charge carriers and bringing down efficiencies^{4,5}. It is known from Shockley-Read-Hall theory that defect trap states placed in the middle of the band gap have a very high trapping rate of charge carriers as opposed to shallow defect states⁸. On the other hand, such deep levels could also be entangled for quantum sensing or lead to increased absorption of sub-gap energy photons by creating intermediate band PVs⁹⁻¹⁷. The experimental determination of the presence, the type and the origin of defects in semiconductors, e.g. via cathodoluminescence (CL) or deep level transient spectroscopy (DLTS), is non-trivial^{18,19}. First principles-based density functional theory (DFT) computations provide a useful methodology to study defects, and have been widely applied to accurately predict the defects formation energy and charge transition levels for a large number of crystalline materials^{2,20,21}.

Methylammonium lead halide perovskites with the general

formula MAPbX_3 ($X = \text{I}/\text{Br}/\text{Cl}$) have been extensively studied in the last decade or so for optoelectronic applications²²⁻³³. The possibility of doping at MA or Pb sites as well as halogen site mixing provides a large playground for the tuning of electronic structure, absorption coefficients, and defect properties in the MAPbX_3 family of perovskites³⁴⁻⁴³. Recently, we performed a comprehensive study of partial Pb substitution in MAPbBr_3 and discovered that a number of transition metals lead to low energy Pb-site defects, are capable of shifting the equilibrium Fermi level and thus the nature of conductivity, and create energy states in the band gap¹⁶. Further, it is seen that mixed halide perovskites have band gaps intermediate to the parent perovskites' band gaps. Mixing of halogen atoms in perovskites has frequently been used to tailor electronic structure, charge transfer and carrier lifetimes⁴⁴⁻⁴⁹. Partial substitution of I by Br has been shown to enhance the photoinduced halide segregation and charge carrier recombination in MAPbI_3 , as well as shift certain defect energy levels⁵⁰⁻⁵².

It has been reported in the past that both MAPbI_3 and MAPbBr_3 , the two most commonly used halide perovskites, have impressively high defect tolerance^{31,54,55}, and owe their utility as PV semiconductors to their optoelectronically benign defects. However, composition engineering at the halogen site can lead to new perovskites where the same defects are no longer benign. Not only can certain defects and impurities become more energetically favorable in mixed halide perovskites (as opposed to pure halides), they could create deeper energy levels and thus have a notable influence on the optoelectronic behavior. Mixed iodide-bromide or bromide-chloride perovskites could be preferred for certain applications due to thermodynamic reasons, availability of precursors, band gap engineering, or other experimental concerns. It is vital to understand the behavior of prominent point defects in such compounds, as well as to screen for

^{a)}Electronic mail: mannodi@anl.gov

^{b)}Electronic mail: mchan@anl.gov

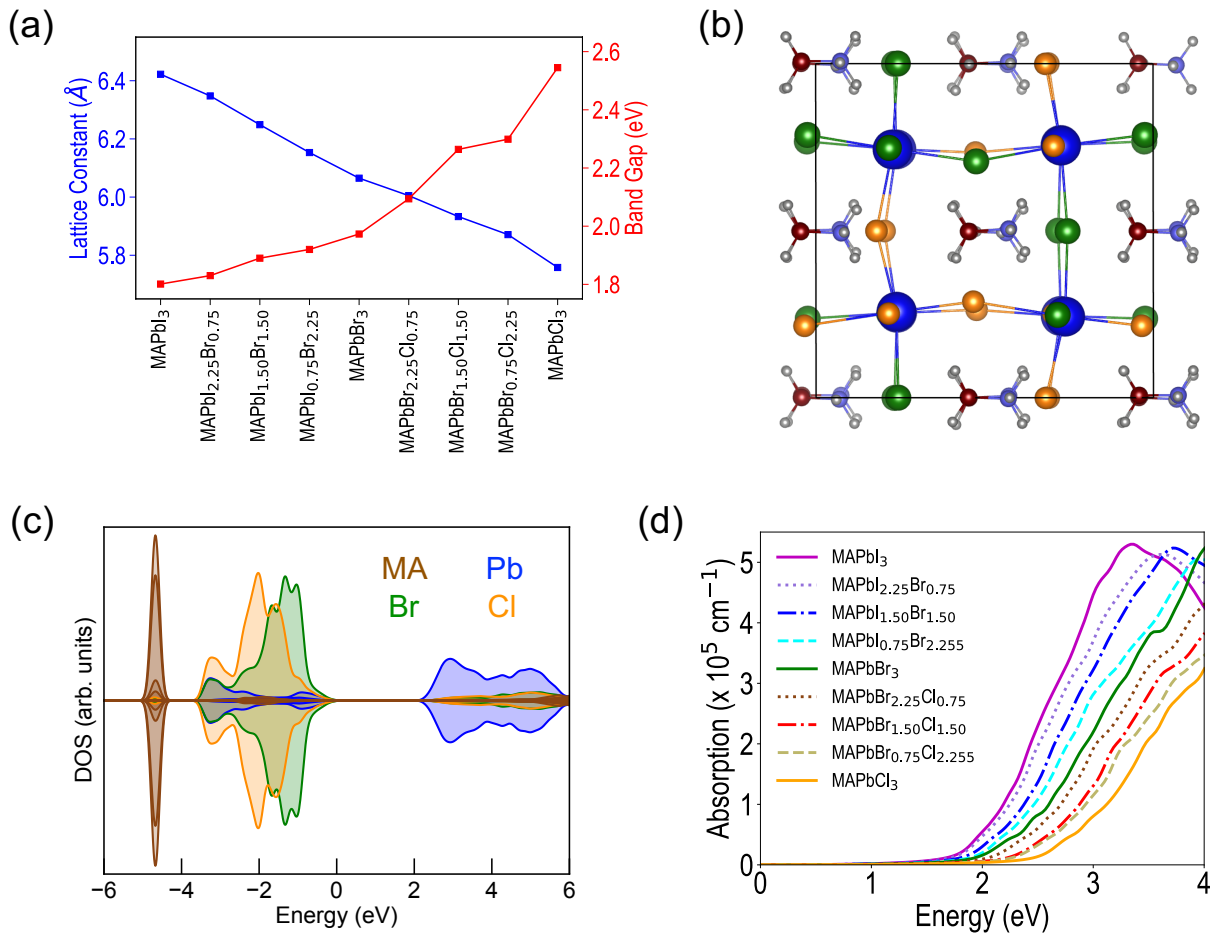


FIG. 1: (a) DFT computed lattice constant and band gap variation for different perovskite compositions from MAPbI₃ to mixed iodide-bromide to mixed bromide-chloride to MAPbCl₃. Lattice constant uniformly decreases from iodide to chloride whereas band gap increases. (b) Optimized pseudo-cubic structure of perovskite MAPbBr_{1.5}Cl_{1.5} shown as an example. Pb is shown in blue, Br in green, Cl in orange, C in dark red, N in purple and H in silver. (c) Computed density of states for MAPbI_{1.5}Br_{1.5}. There is uniform mixing between Br and Cl energy states near the valence band maximum. (d) Computed absorption spectra for the 9 perovskites, from MAPbI₃ to MAPbCl₃. Absorption onset gets delayed moving from iodide to chloride owing to the increase in band gap, but absorption coefficient magnitude follows the trend MAPbI₃ > MAPbBr₃ > MAPbCl₃. (c) and (d) computed using Sumo⁵³.

possible impurities that could be present in the material or indeed, be incorporated (e.g., at the Pb-site) to affect a certain change in the equilibrium conductivity.

In this work, we simulate the structures of several mixed iodide-bromide and bromide-chloride hybrid perovskites and apply density functional theory (DFT) computations to obtain a clear picture of the defect physics in each. We compare the electronic structure and defect properties, specifically the energetics and charge transition levels of dominant point defects, in 9 perovskite systems—MAPbI₃, MAPbBr₃, MAPbCl₃, MAPbI_{3-y}Br_y and MAPbBr_{3-y}Cl_y ($y = 2.25, 1.50, 0.75$). Under ambient conditions, MAPbBr₃ and MAPbCl₃ are expected to crystallize in the cubic phase whereas MAPbI₃ adopts the tetragonal phase⁵⁶⁻⁶¹. However, for simplicity of comparison and for ease of simulation of

mixed halide systems, we use the pseudo-cubic crystal structures for each perovskite, with computed lattice constants of $a = 5.76 \text{ \AA}$ (MAPbCl₃), $a = 6.07 \text{ \AA}$ (MAPbBr₃) and $a = 6.42 \text{ \AA}$ (MAPbI₃). The mixed halide perovskites were simulated by generating special quasi-random structures (SQS)^{62,63} starting from the $2 \times 2 \times 2$ supercells of MAPbI₃ and MAPbBr₃. The pseudo-cubic lattice constants and band gaps computed at the PBE level of theory for all 9 perovskites are shown in Fig. 1 (a) and listed in Table SII along with measured values from the literature^{15,56-61}. The optimized structure of MAPbBr_{1.5}Cl_{1.5} (50-50 solid solution of Br-Cl) is shown in Fig. 1 (b) as an example.

It can be seen that going from MAPbI₃ to MAPbCl₃, the lattice constant steadily decreases whereas the band gap steadily rises from $\sim 1.80 \text{ eV}$ to $\sim 2.55 \text{ eV}$, values that are

higher (lower) than reported experimental results for MAPbI₃ (MAPbCl₃). The structures of all 9 simulated perovskites are shown in Fig. S11. The energy of formation of any mixed halide perovskite against decomposition to pure perovskites is computed to be less than 15 meV per formula unit, indicating their robust stability; these computed energies are listed in Table S11. The mixed I-Cl perovskites have energy of formation > 150 meV per formula unit¹⁷, and were thus not considered for this study. In Fig. 1 (c), we have plotted the computed density of states (DOS) of MAPbBr_{1.5}Cl_{1.5}, showing that while the conduction band minimum (CBM) is dominated by Pb energy states, the (mixed) halogen energy states determine the valence band maximum (VBM). The computed DOS of all 9 perovskites are plotted in Fig. S12. Lastly, Fig. 1 (d) shows the computed absorption spectra of all 9 perovskites, showing clear increasing and decreasing trends, respectively, in the onset of absorption and magnitude of absorption coefficient (y-axis) on going from MAPbI₃ to MAPbCl₃. The continuous tunability of lattice, optical and electronic structure properties as a function of composition, combined with the reasonable energetic stability, confirms the mixed halide perovskites as a fertile space for designing materials for tailored electronic properties.

All DFT computations were performed using the Vienna ab-initio software package (VASP), applying the generalized gradient approximation (GGA) parametrized by Perdew, Burke and Ernzerhof (PBE) and using the projector-augmented wave (PAW) pseudopotentials. The plane wave energy cut-off was set at 500 eV and all atomic structures were fully relaxed until forces on all atoms were less than 0.05 eV/Å. Every calculation for structure optimization, density of states, and simulation of point defects was performed on a 96 atom 2x2x2 perovskite supercell. While trends in lattice constants, band gaps and defect levels are correctly captured when compared to available experiments, deviations arise because of limitations of using a semilocal functional, as well as the neglect of spin-orbit coupling (SOC). Band gaps, band edges and defect energies can be further corrected by the inclusion of SOC³³ and hybrid functionals (e.g. HSE06⁶⁴) or GW corrections⁶⁵. However, we stick to the PBE functional for ease of computation and because properties and trends computed in the past using the same approximations provided a very good qualitative picture of the electronic and defect properties of hybrid perovskites^{15,16}. Our recent work¹⁶ shows that corrections from SOC and HSE06 cancel each other out, resulting in a good comparison of PBE computed (without SOC) band gaps and defect levels with measured quantities. The supercell size and the orientation of the MA molecules are other potential sources of errors that are ignored here.

For defect calculations, we simulated vacancy, interstitial and substitutional (self and extrinsic) defects in every 96 atom supercell, and optimized the defect structures in various charge states to calculate defect formation energies as a function of the total charge and the chemical potentials of different species, including the electrons. Equation 1 is used to calcu-

late the formation energy of any point defect in a perovskite MAPbX₃-

$$E^f(D^q, E_F) = E(D^q) - 8E(\text{MAPbX}_3) - \mu_D + qE_F + E_{corr} \quad (1)$$

Here, $E(D^q)$ is the total DFT energy of the defect containing supercell in a charge state q , $E(\text{MAPbX}_3)$ is the total DFT energy of one formula unit of the bulk perovskite, μ_D is the chemical potential of the relevant species involved in creating the defect, the Fermi level E_F is the electron chemical potential referenced to the VBM of bulk MAPbX₃, and E_{corr} is the correction energy term calculated using Freysoldt's correction scheme^{20,21} to account for periodic interaction between the charge and its image. Defect charge transition levels are defined as the E_F values where the defect transitions from one stable charged state to another; such levels would correspond to defect states relative to the semiconductor band edges. Chemical potential values are selected from the calculated ranges of stability for every perovskite based on the formation energies of the perovskite and the halide compounds of Pb and MA; this has been shown for MAPbCl₃ and MAPbBr₃ in Fig. S13. Before moving to extrinsic substitutional defects, we simulated all possible intrinsic point defects in each of the 9 perovskite systems, namely vacancy (V_{Pb} , V_{MA} , V_I , V_{Br} and V_{Cl}), self-interstitial (Pb_i , MA_i , I_i , Br_i and Cl_i) and anti-site (Pb_{MA} , MA_{Pb} , Pb_I , Pb_{Br} , Pb_{Cl} , MA_I , MA_{Br} , MA_{Cl} , I_{Pb} , I_{MA} , Br_{Pb} , Br_{MA} , Cl_{Pb} and Cl_{MA}) defects. We calculate the charge and Fermi level dependent formation energy of each defect at Pb-rich, halogen-rich and moderate chemical potential conditions.

The Fermi level (E_F) dependent formation energies for the low energy intrinsic defects in the 9 perovskite compounds are plotted for Pb-rich chemical potential conditions in Fig. 2, as E_F moves from VBM to CBM. The complete formation energies for Pb-rich, moderate and halogen-rich chemical potential conditions are shown in Fig. S14–S112. The first observation is that each of the vacancy defects, namely V_{Pb} , V_{MA} and V_X ($X=I/Br/Cl$), along with the Pb on MA anti-site defect, Pb_{MA} , form the set of intrinsic point defects with lowest formation energies in every system. All the remaining anti-site and interstitial defects have higher formation energies, as seen from Fig. S14–S112, and are less likely to occur or affect the equilibrium opto-electronic properties of the semiconductor than the defects pictured in Fig. 2. It is seen that although the acceptor type defects V_{Pb} ($q = -2$) and V_{MA} ($q = -1$) and the donor type defects V_X ($q = +1$) and Pb_{MA} ($q = +1$) all occur in their expected charge states for the majority of the band gap region, there are many cases where these defects show charge transition levels within the band gap. We define any transition level that occurs at a Fermi level > 0.2 eV away from the VBM or the CBM as a "deep" defect level, while the transition levels close to the band edges are termed "shallow".

We observe from Fig. 2 (a), (b), (c), (d) and (e) that in MAPbI₃, MAPbBr₃ and each of the iodide-bromide perovskites, the low energy defects create only shallow transition

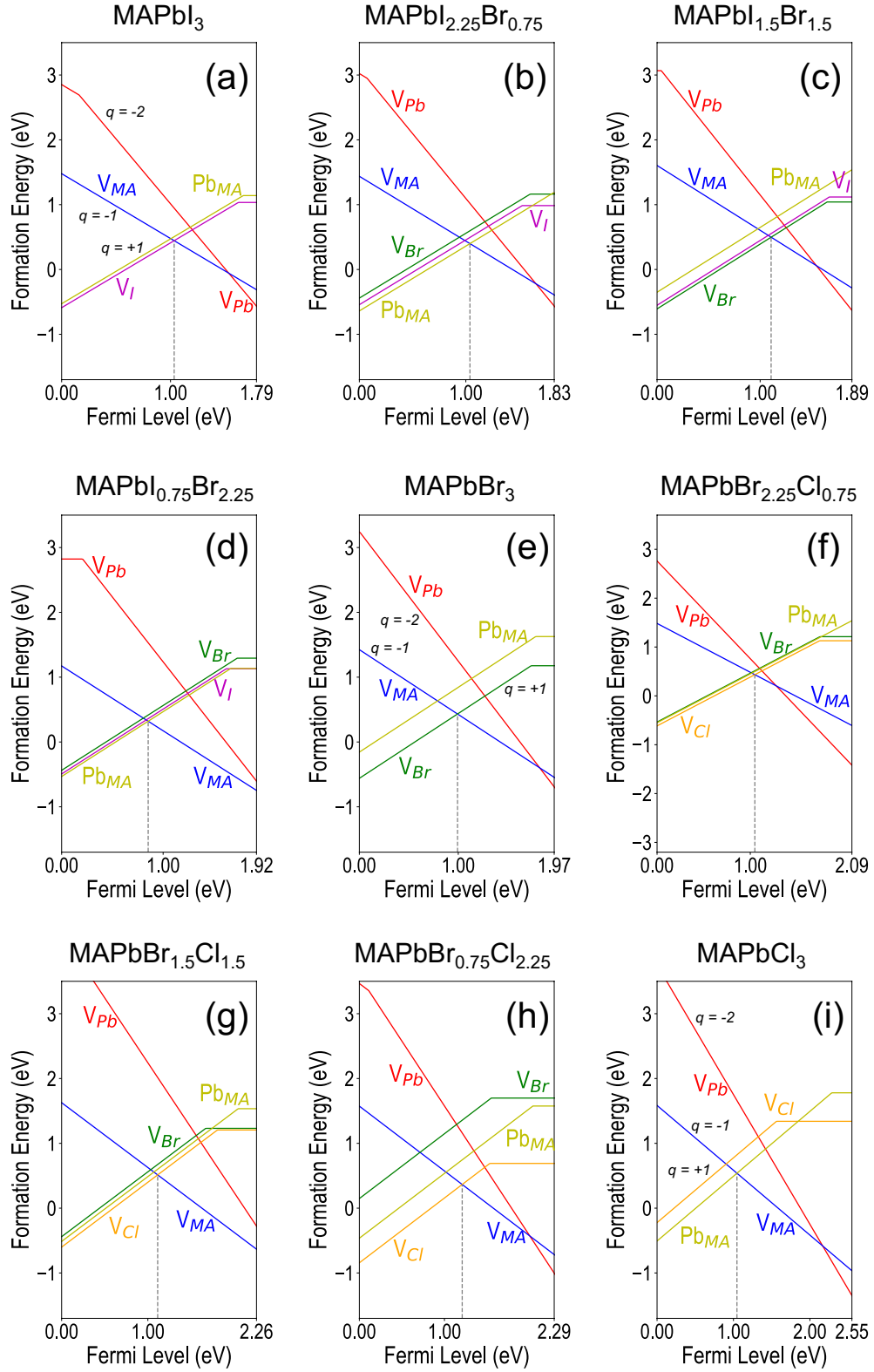


FIG. 2: Calculated formation energies of intrinsic point defects under Pb-rich chemical potential conditions in (a) $MAPbI_3$, (b) $MAPbI_{2.25}Br_{0.75}$, (c) $MAPbI_{1.5}Br_{1.5}$, (d) $MAPbI_{0.75}Br_{2.25}$, (e) $MAPbBr_3$, (f) $MAPbBr_{2.25}Cl_{0.75}$, (g) $MAPbBr_{1.5}Cl_{1.5}$, (h) $MAPbBr_{0.75}Cl_{2.25}$ and (i) $MAPbCl_3$.

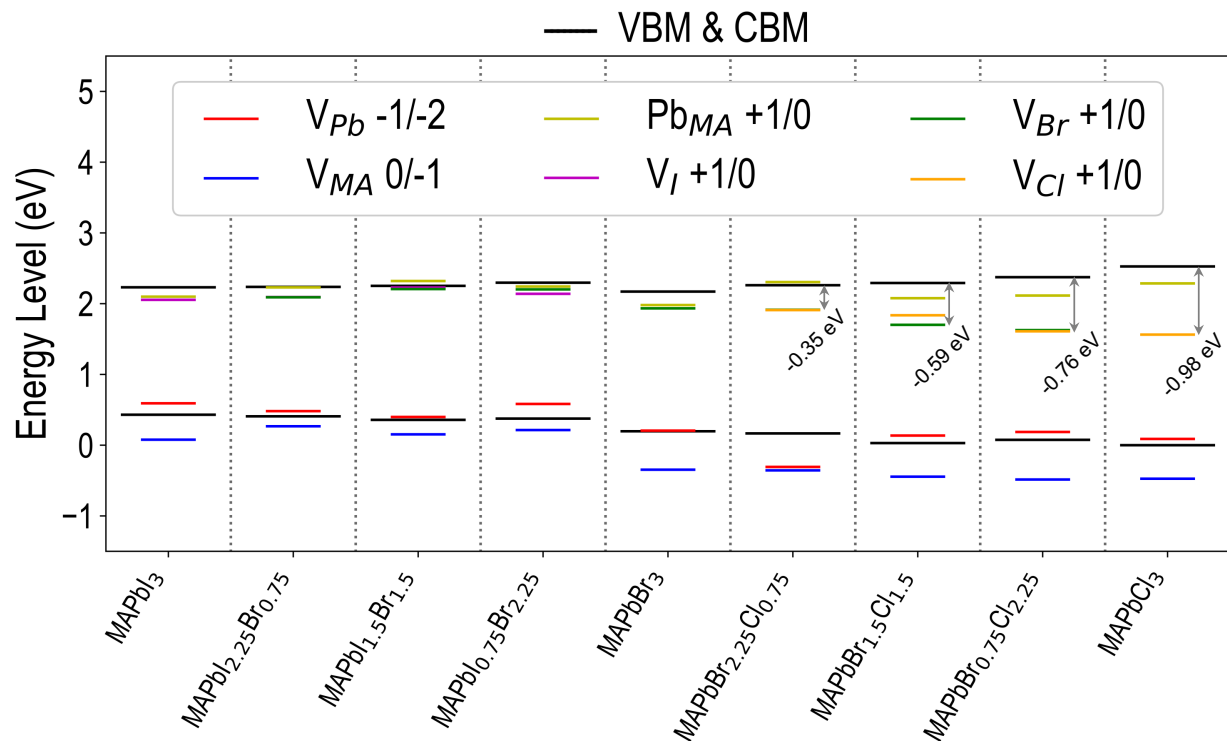


FIG. 3: Relevant charge transition levels of dominant intrinsic defects in the 9 perovskites. $\text{MAPbI}_{3-y}\text{Br}_y$ compounds show only shallow defect transition levels, whereas the halogen vacancy (V_{Br} and V_{Cl}) +1/0 transition level becomes deeper in the band gap for Cl-containing perovskites. Energy levels are aligned using the Nitrogen core 1s state energy from each calculation.

levels, such as the V_I or V_{Br} +1/0 transition, or the V_{Pb} -1/-2 transition. While V_{MA} is the lowest energy acceptor type defect, V_I , V_{Br} and Pb_{MA} all have similar low energies and alternate as the dominant donor type defect. This is consistent with reports that suggest perovskites like MAPbI_3 have a tendency to release MAI through the formation of vacancy couples, V_{MA} and V_I , which has negligible impact on the photoluminescence properties⁵⁴. For every MAPbX_3 compound, the equilibrium Fermi level E_F^{eqm} , which is determined by charge neutrality conditions⁶⁶ and roughly indicated in Fig. 2 by dashed vertical lines, goes from strongly p-type (inside the VB) for halogen-rich conditions to moderately p-type for moderate chemical potential to intrinsic (middle of the band gap) for Pb-rich conditions, as shown in Fig. SI4–SI12 and in Fig. 2. The equilibrium conductivity of any perovskite can be tailored by the growth conditions, and different impurities can induce a p-type or n-type shift based on the chemical potential, as will be explained later.

In contrast to the $\text{MAPbI}_{3-y}\text{Br}_y$ ($y = 0, 0.75, 1.5, 2.25, 3$) perovskites which don't show deep defect levels, the Cl-containing $\text{MAPbBr}_{3-y}\text{Cl}_y$ ($y = 0.75, 1.5, 2.25, 3$) perovskites show halogen vacancy defect states that go deeper in the band gap with increasing concentration of Cl in the perovskite. As shown in Fig. 2 (f), (g), (h) and (i), the V_{Br} and V_{Cl} +1/0 transition levels occur at > 0.2 eV from the CBM for each of the Cl-containing perovskites, becoming deeper from (f) to (i). This shows that while the halogen vacancies are among

the lowest energy donor defects in all perovskite compositions studied here, and E_F^{eqm} follows the same trend from halogen-rich to Pb-rich conditions, deeper intrinsic defect levels are likely to be present in Cl-containing perovskites. This raises the possibility of non-radiative recombination of charge carriers in pure chloride and mixed bromide-chloride perovskites which could lead to lower carrier lifetimes, diffusion lengths and power conversion efficiencies (PCE). While there have been reports of improvement in carrier lifetimes and diffusion lengths upon addition of small amounts of Br or Cl to pure iodide-based solar cells^{60,67–69}, the highest PCEs are achieved for I-rich perovskites^{70,71}. The general lack of success of pure chloride and mixed bromide-chloride perovskite solar cells can be attributed to the low energy deep defects in Cl-rich compositions, and makes these wider band gap semiconductors more suitable for tandem solar cells^{72,73} and intermediate band PVs^{15,17}.

In Fig. 3, we plotted some of the relevant charge transition levels of low energy defects, namely V_{Pb} (-1/-2), V_{MA} (0/-1), Pb_{MA} (+1/0), V_I (+1/0), V_{Br} (+1/0) and V_{Cl} (+1/0), computed across the 9 perovskite compounds. Each transition level as well as the respective perovskite VBM and CBM are plotted alongside each other by referencing all energy levels to the deep nitrogen 1s core state energy from each calculation, with the MAPbCl_3 VBM set to energy = 0 eV. It can be seen that the V_{Pb} (-1/-2), V_{MA} (0/-1) and Pb_{MA} (+1/0) levels occur close enough to the VBM or CBM to be regarded as

TABLE I: The elements studied here as extrinsic substituents at the Pb site, the ionic radii for their relevant oxidation states, and their tolerance and octahedral factors in a Bromide and Chloride perovskite lattice.

Element	Ox. State	Ionic Radius (pm)	$t(\text{MAMBr}_3)$	$\mu(\text{MAMBr}_3)$	$t(\text{MAMCl}_3)$	$\mu(\text{MAMCl}_3)$
Pb	+2	133	0.808	0.679	0.813	0.735
Sc	+3	88.5	0.935	0.452	0.947	0.489
Ti	+3	81	0.960	0.413	0.974	0.448
Co	+2	88.5	0.935	0.452	0.947	0.489
Cu	+1	91	0.926	0.464	0.938	0.503
Y	+3	104	0.886	0.531	0.896	0.575
Zr	+4	86	0.943	0.439	0.956	0.475
Nb	+3	86	0.943	0.439	0.956	0.475
Mo	+3	83	0.953	0.423	0.967	0.459
Hf	+4	85	0.946	0.434	0.960	0.470
In	+3	94	0.917	0.480	0.928	0.519
Tl	+3	102.5	0.891	0.523	0.900	0.566
Sn	+4	83	0.953	0.423	0.967	0.459
Sb	+3	90	0.930	0.459	0.942	0.497
Bi	+3	117	0.849	0.597	0.857	0.646

shallow defect levels across the 9 perovskites. V_I (+1/0) and V_{Br} (+1/0) are also shallow levels in the $\text{MAPbI}_{3-y}\text{Br}_y$ ($y = 0, 0.75, 1.5, 2.25, 3$) perovskites. The V_{Br} (+1/0) and V_{Cl} (+1/0) both become visibly deeper with increasing y in $\text{MAPbBr}_{3-y}\text{Cl}_y$ perovskites, going from 0.35 eV below CBM to 0.59 eV to 0.76 eV and to nearly 1 eV in MAPbCl_3 . To summarize, DFT computations reveal that halogen vacancy defect levels are shallow in iodine containing perovskites but deep in chlorine containing perovskites.

Impurity atoms or extrinsic point defects can be introduced in a semiconductor to potentially modify the defect or electronic properties as determined by the dominant intrinsic defects. If an extrinsic impurity creates a lower energy acceptor or donor type defect than the lowest energy intrinsic acceptor or donor type defects, respectively, the dominant intrinsic defect(s) can be compensated for, as the equilibrium Fermi level will be changed. We studied this effect by considering several extrinsic substitutional impurities at the Pb site in three perovskites: MAPbBr_3 , $\text{MAPbBr}_{1.5}\text{Cl}_{1.5}$ and MAPbCl_3 , and comparing their computed defect formation energies to the intrinsic defect energetics. In a recently published study¹⁶, we performed an extensive computational study of nearly all period II, III, IV, V and VI elements as substitutional impurities at the Pb site in MAPbBr_3 , and obtained a list of substituents (mainly some transition metals) that create low energy defects and change the equilibrium Fermi level in the perovskite. We present the same results here for MAPbBr_3 , and extend the study to a set of selected substituents in $\text{MAPbBr}_{1.5}\text{Cl}_{1.5}$ and MAPbCl_3 .

In order to determine suitable substitutional impurity atoms for a given perovskite, the Goldschmidt tolerance and octahedral factors⁷⁴ provide a reasonable estimate of the structural stability of the atom in the perovskite environment. Stable halide perovskites are known to possess tolerance and octahedral factors in the ranges ~ 0.8 – 1.1 and ~ 0.44 – 0.9 ,

respectively¹⁵. Using these criteria, we determine a set of suitable substituents that are listed in Table I, along with their stable oxidation states, ionic radii, and tolerance and octahedral factors in the bromide and chloride perovskite lattices. We performed computations on M_{Pb} substitutional defects in different charged states in MAPbBr_3 , $\text{MAPbBr}_{1.5}\text{Cl}_{1.5}$ and MAPbCl_3 , where M is one of the 15 elements shown in Table I. The Fermi level dependent formation energies were computed as before, and we plotted the formation energies for all the low energy extrinsic defects along with the low energy intrinsic defects for halogen-rich, moderate and Pb-rich chemical potential conditions for MAPbBr_3 in Figure SI13 (reproduced from ref.¹⁶), and $\text{MAPbBr}_{1.5}\text{Cl}_{1.5}$ and MAPbCl_3 in Fig. 4.

It is seen that transition metals have the most interesting behavior as extrinsic impurities in the perovskites, with several of them creating low energy donor type defects that dominate over V_{Br} and V_{Cl} . Most of the transition metals prefer oxidation states of +3 or +4, which leads to a net positive charge in the system when they replace the +2 oxidation state Pb atom, explaining why they create donor type defects. Sc, Zr, Nb, Mo and Hf are the low energy impurity atoms in MAPbBr_3 under different chemical potential conditions, as plotted in Fig. SI13. Fig. 4 (a) shows that Y and Mo are the only low energy impurities in $\text{MAPbBr}_{1.5}\text{Cl}_{1.5}$ but have comparable energetics to the dominant donor type intrinsic defect Pb_{MA} , while from Fig. 4 (b), it is seen that Y, Zr, Nb and Hf all create low formation energy extrinsic defects in MAPbCl_3 . Each of these stable impurities in each perovskite would move E_F^{eqm} to the right and make the conductivity slightly more n-type; this has been shown in Fig. 4 (b) for Y_{Pb} in MAPbCl_3 , with very p-type, moderate p-type and intrinsic conductivity resulting in Cl-rich, moderate and Pb-rich conditions, respectively.

It can be concluded that a few transition metals such as Sc,

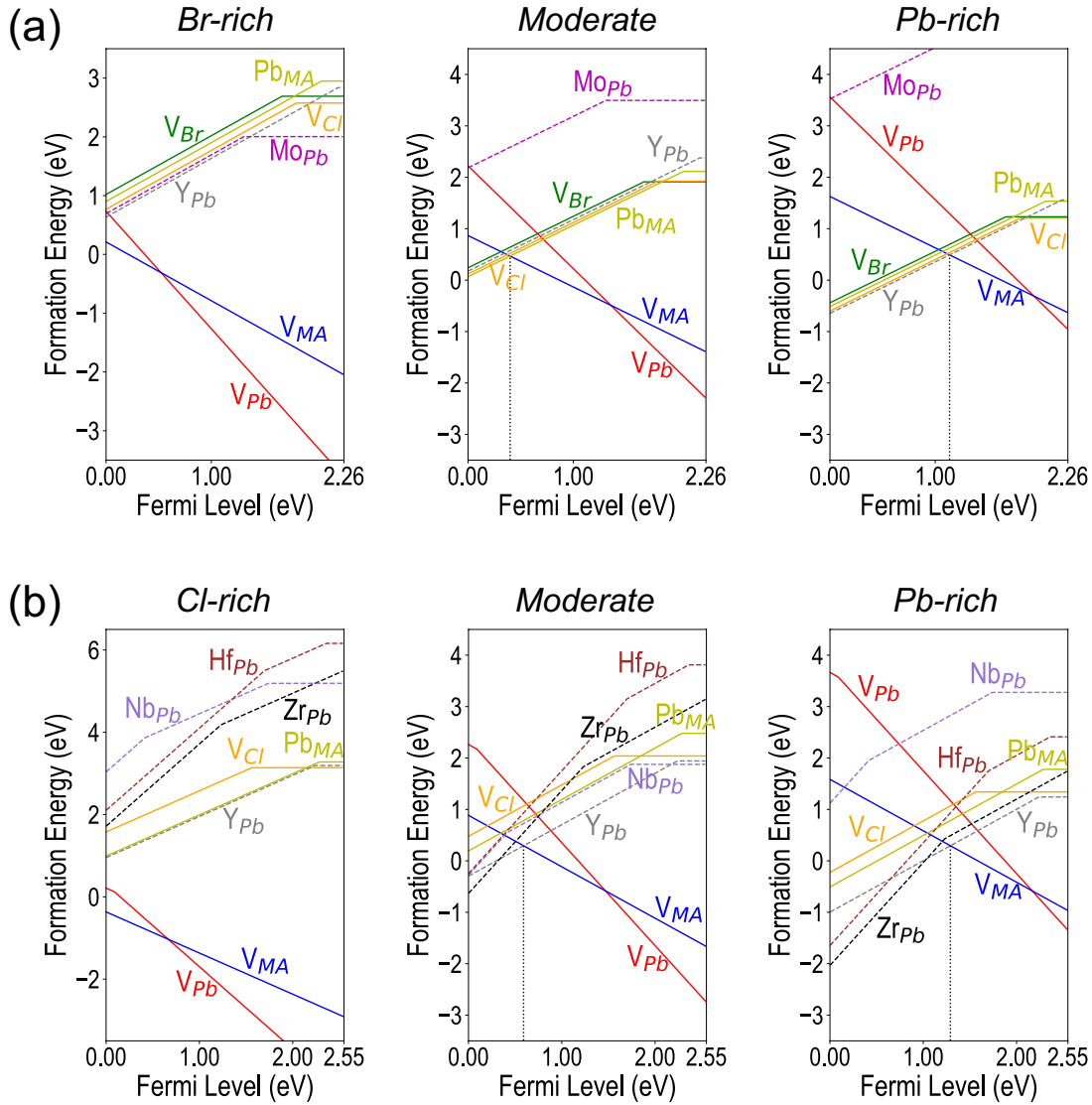


FIG. 4: Computed formation energies of extrinsic substitutional defects in (a) $\text{MAPbBr}_{1.5}\text{Cl}_{1.5}$ and (b) MAPbCl_3 .

Zr and Hf can potentially create low formation energy donor type defects in bromide, chloride or mixed bromide-chloride perovskites when substituting a Pb atom. However, it should also be noticed that many of these extrinsic defects show deep charge transition levels, owing to the stability of the transition metal in multiple charge states. A comparison between the $+2/+1$ or $+1/0$ transition levels of a few selected substitutional impurities are shown in Fig. 5 for MAPbBr_3 , $\text{MAPbBr}_{1.5}\text{Cl}_{1.5}$ and MAPbCl_3 . Certain levels that are deep in one compound can be pushed closer to the VBM or CBM in others; for example, the Nb_{Pb} $+2/+1$ level that occurs around the middle of the MAPbBr_3 band gap is pretty shallow in $\text{MAPbBr}_{1.5}\text{Cl}_{1.5}$ and MAPbCl_3 . The Sc_{Pb} and Mo_{Pb} $+1/0$ levels, on the other hand, are much deeper in $\text{MAPbBr}_{1.5}\text{Cl}_{1.5}$ and MAPbCl_3 , and will be considered shallow in MAPbBr_3 .

Mid-gap impurity transition levels raise the same concern

as before of a detrimental effect on PV performance due to non-radiative recombination of carriers. But recent studies by our group and some others have raised the promise of intermediate band photovoltaics functioning via sub-gap photon absorption induced by half-filled impurity energy levels in the band gap^{15–17}. Such levels can both accept electrons from the valence band and emit them to the conduction band, creating a 2 step photon absorption process which can theoretically increase the solar cell efficiency. The discovery of low energy deep defect creating impurities in halide perovskites thus becomes significant, and could potentially be incorporated and tested in real solar cell materials. We experimentally studied a few such substituents (including Zr) in MAPbBr_3 as part of our recent work¹⁶, but were unable to conclusively provide evidence of sub-gap absorption. Nevertheless, a complete computational picture of intrinsic and extrinsic defects in halide perovskites as obtained in this work provides

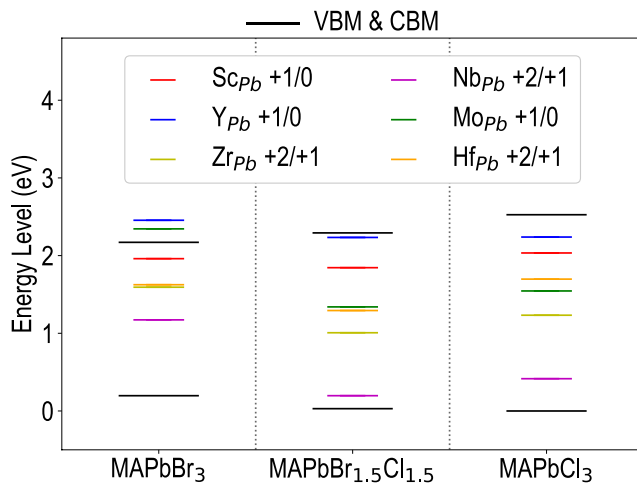


FIG. 5: Computed charge transition levels of extrinsic defects in MAPbBr₃, MAPbBr_{1.5}Cl_{1.5} and MAPbCl₃.

us with a list of possible substituents that can be introduced in bromide or mixed bromide-chloride perovskites of various compositions to suitably change the defect and electronic properties for PV applications.

In summary, we used first principles computations to study the trends in defect formation energies, defect energy levels and equilibrium Fermi level for various types of point defects in different compositions of pseudo-cubic methylammonium lead halide perovskites. We observed that the lowest energy intrinsic defects, namely the vacancy defects and Pb on MA anti-site defect, only create shallow levels in the iodide, bromide and mixed iodide-bromide perovskites, but create deeper levels in the pure chloride and mixed bromide-chloride perovskites, which could be unfavorable due to the danger of non-radiative recombination of charge carriers. We further studied several extrinsic substitutional impurities at the Pb-site in three perovskites, MAPbBr₃, MAPbBr_{1.5}Cl_{1.5} and MAPbCl₃, and discovered that certain transition metals like Sc, Zr, Hf, Mo and Y can create donor type defects with lower energy than the potentially deep level creating halogen vacancy defects. Such impurities can dominate over the intrinsic defects and change the nature of conductivity in the perovskite, while themselves creating energy levels in the band gap that can potentially be exploited for sub-gap absorption and increased PV efficiencies.

This material is based upon work supported by Laboratory Directed Research and Development (LDRD) funding from Argonne National Laboratory, provided by the Director, Office of Science, of the U.S. Department of Energy under Contract No. DE-AC02-06CH11357. Use of the Center for Nanoscale Materials, an Office of Science user facility, was supported by the U.S. Department of Energy, Office of Science, Office of Basic Energy Sciences, under Contract No. DE-AC02-06CH11357. This research used resources of the National Energy Research Scientific Computing Center

(NERSC), a DOE Office of Science User Facility supported by the Office of Science of the U.S. Department of Energy under Contract No. DE-AC02-05CH11231. We gratefully acknowledge the computing resources provided on Blues and Bebop, high-performance computing clusters operated by the Laboratory Computing Resource Center (LCRC) at Argonne National Laboratory.

REFERENCES

- H. J. Queisser and E. E. Haller, "Defects in semiconductors: Some fatal, some vital," *Science* **281**, 945–950 (1998), <http://science.sciencemag.org/content/281/5379/945.full.pdf>.
- P. A. Schultz, "Theory of defect levels and the "band gap problem" in silicon," *Phys. Rev. Lett.* **96**, 246401 (2006).
- D. Krasikov and I. Sankin, "Defect interactions and the role of complexes in the cdtc solar cell absorber," *J. Mater. Chem. A* **5**, 3503–3513 (2017).
- S. Kim, J.-S. Park, and A. Walsh, "Identification of killer defects in kesterite thin-film solar cells," *ACS Energy Letters* **3**, 496–500 (2018), <https://doi.org/10.1021/acsenenergylett.7b01313>.
- W.-J. Yin, T. Shi, and Y. Yan, "Unusual defect physics in ch₃nh₃pb₃i₃ perovskite solar cell absorber," *Applied Physics Letters* **104**, 063903 (2014), <https://doi.org/10.1063/1.4864778>.
- T. Shi, W.-J. Yin, F. Hong, K. Zhu, and Y. Yan, "Unipolar self-doping behavior in perovskite ch₃nh₃pb₃r₃," *Applied Physics Letters* **106**, 103902 (2015), <https://doi.org/10.1063/1.4914544>.
- J. S. Park, S. Kim, Z. Xie, and A. Walsh, "Point defect engineering in thin-film solar cells," *Nature Reviews Materials* **2058-8437** (2018), 10.1038/s41578-018-0026-7.
- D. Meggiolaro and F. De Angelis, "First-principles modeling of defects in lead halide perovskites: Best practices and open issues," *ACS Energy Letters* **3**, 2206–2222 (2018), <https://doi.org/10.1021/acsenenergylett.8b01212>.
- A. Luque and A. Martí, "Increasing the efficiency of ideal solar cells by photon induced transitions at intermediate levels," *Phys. Rev. Lett.* **78**, 5014–5017 (1997).
- A. Luque, A. Martí, and C. Stanley, "Understanding intermediate-band solar cells," *Nature Photonics* **6**, 146–152 (2012).
- A. Martí, E. Antolín, C. R. Stanley, C. D. Farmer, N. López, P. Díaz, E. Cánovas, P. G. Linares, and A. Luque, "Production of photocurrent due to intermediate-to-conduction-band transitions: A demonstration of a key operating principle of the intermediate-band solar cell," *Phys. Rev. Lett.* **97**, 247701 (2006).
- S. Sonoda, "Partially filled intermediate band of cr-doped gan films," *Applied Physics Letters* **100**, 202101 (2012), <https://doi.org/10.1063/1.4717716>.
- P. Wahnón and C. Tablero, "Ab initio electronic structure calculations for metallic intermediate band formation in photovoltaic materials," *Phys. Rev. B* **65**, 165115 (2002).
- Y. Okada, N. J. Ekins-Daukes, T. Kita, R. Tamaki, M. Yoshida, A. Pusch, O. Hess, C. C. Phillips, D. J. Farrell, K. Yoshida, N. Ahsan, Y. Shoji, T. Sogabe, and J.-F. Guillemoles, "Intermediate band solar cells: Recent progress and future directions," *Applied Physics Reviews* **2**, 021302 (2015), <https://doi.org/10.1063/1.4916561>.
- M. D. Sampson, J. S. Park, R. D. Schaller, M. K. Y. Chan, and A. B. F. Martinson, "Transition metal-substituted lead halide perovskite absorbers," *J. Mater. Chem. A* **5**, 3578–3588 (2017).
- A. Mannodi-Kanakithodi, J.-S. Park, N. Jeon, D. H. Cao, D. J. Gosztola, A. B. F. Martinson, and M. K. Y. Chan, "Comprehensive computational study of partial lead substitution in methylammonium lead bromide," *Chemistry of Materials* **31**, 3599–3612 (2019), <https://doi.org/10.1021/acscemmater.8b04017>.
- D. H. Cao, P. Guo, A. Mannodi-Kanakithodi, G. P. Wiederrecht, D. J. Gosztola, N. Jeon, R. D. Schaller, M. K. Y. Chan, and A. B. F. Martinson, "Charge transfer dynamics of phase-segregated halide perovskites: Ch₃nh₃pb₃l₃ and ch₃nh₃pb₃i₃ or (c₄h₉nh₃)₂(ch₃nh₃)₃na₂l₅i₃pb₃ni₃n+1 mix

- tures,” *ACS Applied Materials & Interfaces* **11**, 9583–9593 (2019), <https://doi.org/10.1021/acsami.8b20928>.
- ¹⁸S. Heo, G. Seo, Y. Lee, D. Lee, M. Seol, J. Lee, J.-B. Park, K. Kim, D.-J. Yun, Y. S. Kim, J. K. Shin, T. K. Ahn, and M. K. Nazeeruddin, “Deep level trapped defect analysis in $\text{ch}_3\text{nh}_3\text{pb}_3\text{i}_3$ perovskite solar cells by deep level transient spectroscopy,” *Energy Environ. Sci.* **10**, 1128–1133 (2017).
- ¹⁹J. W. Rosenberg, M. J. Legodi, Y. Rakita, D. Cahen, and M. Diale, “Laplace current deep level transient spectroscopy measurements of defect states in methylammonium lead bromide single crystals,” *Journal of Applied Physics* **122**, 145701 (2017), <https://doi.org/10.1063/1.4995970>.
- ²⁰C. Freysoldt, J. Neugebauer, and C. G. Van de Walle, “Fully ab initio finite-size corrections for charged-defect supercell calculations,” *Phys. Rev. Lett.* **102**, 016402 (2009).
- ²¹C. Freysoldt, B. Grabowski, T. Hickel, J. Neugebauer, G. Kresse, A. Janotti, and C. G. Van de Walle, “First-principles calculations for point defects in solids,” *Rev. Mod. Phys.* **86**, 253–305 (2014).
- ²²A. Kojima, K. Teshima, Y. Shirai, and T. Miyasaka, “Organometal halide perovskites as visible-light sensitizers for photovoltaic cells,” *Journal of the American Chemical Society* **131**, 6050–6051 (2009), pMID: 19366264, <https://doi.org/10.1021/ja809598r>.
- ²³J.-H. Im, C.-R. Lee, J.-W. Lee, S.-W. Park, and N.-G. Park, “6.5solar cell,” *Nanoscale* **3**, 4088–4093 (2011).
- ²⁴T. Baikie, Y. Fang, J. M. Kadro, M. Schreyer, F. Wei, S. G. Mhaisalkar, M. Graetzel, and T. J. White, “Synthesis and crystal chemistry of the hybrid perovskite (ch_3nh_3) pb_3i_3 for solid-state sensitised solar cell applications,” *J. Mater. Chem. A* **1**, 5628–5641 (2013).
- ²⁵X. Zhou, J. Jankowska, H. Dong, and O. V. Prezhdo, “Recent theoretical progress in the development of perovskite photovoltaic materials,” *Journal of Energy Chemistry* (2017), <https://doi.org/10.1016/j.jechem.2017.10.010>.
- ²⁶T. M. Brenner, D. A. Egger, L. Kronik, G. Hodes, and D. Cahen, “Hybrid organic–inorganic perovskites: low-cost semiconductors with intriguing charge-transport properties,” *Nature Reviews Materials* **1**, 15007 (2016).
- ²⁷H. Shen, T. Duong, Y. Wu, J. Peng, D. Jacobs, N. Wu, K. Weber, T. White, and K. Catchpole, “Metal halide perovskite: a game-changer for photovoltaics and solar devices via a tandem design,” *Science and Technology of Advanced Materials* **19**, 53–75 (2018), <https://doi.org/10.1080/14686996.2017.1422365>.
- ²⁸J. S. Manser, J. A. Christians, and P. V. Kamat, “Intriguing optoelectronic properties of metal halide perovskites,” *Chemical Reviews* **116**, 12956–13008 (2016), pMID: 27327168, <https://doi.org/10.1021/acs.chemrev.6b00136>.
- ²⁹L. Qiu, L. K. Ono, and Y. Qi, “Advances and challenges to the commercialization of organic–inorganic halide perovskite solar cell technology,” *Materials Today Energy* **7**, 169–189 (2018).
- ³⁰W.-J. Yin, J.-H. Yang, J. Kang, Y. Yan, and S.-H. Wei, “Halide perovskite materials for solar cells: a theoretical review,” *J. Mater. Chem. A* **3**, 8926–8942 (2015).
- ³¹Y. Yan, W.-J. Yin, T. Shi, W. Meng, and C. Feng, “Defect physics of $\text{ch}_3\text{nh}_3\text{pb}_3\text{x}_3$ ($\text{x} = \text{i}, \text{br}, \text{cl}$) perovskites,” in *Organic-Inorganic Halide Perovskite Photovoltaics: From Fundamentals to Device Architectures*, edited by N.-G. Park, M. Grätzel, and T. Miyasaka (Springer International Publishing, Cham, 2016) pp. 79–105.
- ³²C. A. Lpez, M. V. Martnez-Huerta, M. C. Alvarez-Galvn, P. Kayser, P. Gant, A. Castellanos-Gomez, M. T. Fernndez-Daz, F. Fauth, and J. A. Alonso, “Elucidating the methylammonium (ma) conformation in mapbbr_3 perovskite with application in solar cells,” *Inorganic Chemistry* **56**, 14214–14219 (2017), pMID: 29116775, <https://doi.org/10.1021/acs.inorgchem.7b02344>.
- ³³L. D. Whalley, J. M. Frost, Y.-K. Jung, and A. Walsh, “Perspective: Theory and simulation of hybrid halide perovskites,” *The Journal of Chemical Physics* **146**, 220901 (2017), <https://doi.org/10.1063/1.4984964>.
- ³⁴C. Liu, W. Li, J. Fan, and Y. Mai, “A brief review on the lead element substitution in perovskite solar cells,” *Journal of Energy Chemistry* (2017), <https://doi.org/10.1016/j.jechem.2017.10.028>.
- ³⁵J. Gong, P. Guo, S. E. Benjamin, P. G. V. Patten, R. D. Schaller, and T. Xu, “Cation engineering on lead iodide perovskites for stable and high-performance photovoltaic applications,” *Journal of Energy Chemistry* (2017), <https://doi.org/10.1016/j.jechem.2017.12.005>.
- ³⁶Y. Yang, X. Zou, Y. Pei, X. Bai, W. Jin, and D. Chen, “Effect of doping of nai monovalent cation halide on the structural, morphological, optical and optoelectronic properties of mapb_3i_3 perovskite,” *Journal of Materials Science: Materials in Electronics*, **29**, 1–6 (2017).
- ³⁷I. J. Park, S. Seo, M. A. Park, S. Lee, D. H. Kim, K. Zhu, H. Shin, and J. Y. Kim, “Effect of rubidium incorporation on the structural, electrical, and photovoltaic properties of methylammonium lead iodide-based perovskite solar cells,” *ACS Applied Materials & Interfaces* **9**, 41898–41905 (2017), pMID: 29124921, <https://doi.org/10.1021/acsami.7b13947>.
- ³⁸Y. Shirahata and T. Oku, “Photovoltaic properties of cu-doped $\text{ch}_3\text{nh}_3\text{pb}_3\text{i}_3$ with perovskite structure,” *AIP Conference Proceedings* **1807**, 020008 (2017), <https://aip.scitation.org/doi/pdf/10.1063/1.4974790>.
- ³⁹K.-z. Du, X. Wang, Q. Han, Y. Yan, and D. B. Mitzi, “Heterovalent b-site co-alloying approach for halide perovskite bandgap engineering,” *ACS Energy Letters* **2**, 2486–2490 (2017), <https://doi.org/10.1021/acsenenergylett.7b00824>.
- ⁴⁰M. Becker and M. Wark, “Organic cation substitution in hybrid perovskite $\text{ch}_3\text{nh}_3\text{pb}_3\text{i}_3$ with hydroxylammonium (nh_3oh^+): A first-principles study,” *The Journal of Physical Chemistry C* **122**, 3548–3557 (2018), <https://doi.org/10.1021/acs.jpcc.7b10359>.
- ⁴¹M. T. Klug, A. Osherov, A. A. Haghghirad, S. D. Stranks, P. R. Brown, S. Bai, J. T.-W. Wang, X. Dang, V. Bulovic, H. J. Snaith, and A. M. Belcher, “Tailoring metal halide perovskites through metal substitution: influence on photovoltaic and material properties,” *Energy Environ. Sci.* **10**, 236–246 (2017).
- ⁴²J. T.-W. Wang, Z. Wang, S. Pathak, W. Zhang, D. W. deQuilettes, F. Wisnivesky-Rocca-Rivarola, J. Huang, P. K. Nayak, J. B. Patel, H. A. Mohd Yusof, Y. Vaynzof, R. Zhu, I. Ramirez, J. Zhang, C. Ducati, C. Grovenor, M. B. Johnston, D. S. Ginger, R. J. Nicholas, and H. J. Snaith, “Efficient perovskite solar cells by metal ion doping,” *Energy Environ. Sci.* **9**, 2892–2901 (2016).
- ⁴³F. Hao, C. C. Stoumpos, R. P. H. Chang, and M. G. Kanatzidis, “Anomalous band gap behavior in mixed sn and pb perovskites enables broadening of absorption spectrum in solar cells,” *Journal of the American Chemical Society* **136**, 8094–8099 (2014), pMID: 24823301, <https://doi.org/10.1021/ja5033259>.
- ⁴⁴M. A. Mohebbpour, M. Saffari, H. R. Soleimani, and M. B. Tagani, “High performance of mixed halide perovskite solar cells: Role of halogen atom and plasmonic nanoparticles on the ideal current density of cell,” *Physica E: Low-dimensional Systems and Nanostructures* **97**, 282–289 (2018).
- ⁴⁵Z. Xiao, L. Zhao, N. L. Tran, Y. L. Lin, S. H. Silver, R. A. Kerner, N. Yao, A. Kahn, G. D. Scholes, and B. P. Rand, “Mixed-halide perovskites with stabilized bandgaps,” *Nano Letters* **17**, 6863–6869 (2017), pMID: 28968126, <https://doi.org/10.1021/acs.nanolett.7b03179>.
- ⁴⁶H. F. Zariw, N. Soetan, W. R. Erwin, and R. Bardhan, “Mixed halide hybrid perovskites: a paradigm shift in photovoltaics,” *J. Mater. Chem. A* **6**, 5507–5537 (2018).
- ⁴⁷S. Tombe, G. Adam, H. Heilbrunner, D. H. Apaydin, C. Ulbricht, N. S. Sariciftci, C. J. Arendse, E. Iwuoha, and M. C. Scharber, “Optical and electronic properties of mixed halide ($\text{x} = \text{i}, \text{cl}, \text{br}$) methylammonium lead perovskite solar cells,” *J. Mater. Chem. C* **5**, 1714–1723 (2017).
- ⁴⁸X. Wang, Y. Ling, X. Lian, Y. Xin, K. B. Dhungana, F. Perez-Orive, J. Knox, Z. Chen, Y. Zhou, D. Beery, K. Hanson, J. Shi, S. Lin, and H. Gao, “Suppressed phase separation of mixed-halide perovskites confined in endotaxial matrices,” *Nature Communications* **10** (2019), 10.1038/s41467-019-08610-6.
- ⁴⁹D. W. de Quilettes, S. M. Vorpahl, S. D. Stranks, H. Nagaoka, G. E. Eperon, M. E. Ziffer, H. J. Snaith, and D. S. Ginger, “Impact of microstructure on local carrier lifetime in perovskite solar cells,” *Science* **348**, 683–686 (2015), <https://science.sciencemag.org/content/348/6235/683.full.pdf>.
- ⁵⁰E. T. Hoke, D. J. Slotcavage, E. R. Dohner, A. R. Bowring, H. I. Karunadasa, and M. D. McGehee, “Reversible photo-induced trap formation in mixed-halide hybrid perovskites for photovoltaics,” *Chem. Sci.* **6**, 613–617 (2015).
- ⁵¹F. Wang, S. Bai, W. Tress, A. Hagfeldt, and F. Gao, “Defects engineering for high-performance perovskite solar cells,” *npj Flexible Electronics* **2**, 22 (2018).
- ⁵²A. J. Barker, A. Sadhanala, F. Deschler, M. Gandini, S. P. Senanayak, P. M. Pearce, E. Mosconi, A. J. Pearson, Y. Wu, A. R. Srimath Kandada, T. Leijtens, F. De Angelis, S. E. Dutton, A. Petrozza, and R. H. Friend, “Defect-assisted photoinduced halide segregation in mixed-halide perovskite thin

- films,” *ACS Energy Letters* **2**, 1416–1424 (2017).
- ⁵³A. M. Ganose, A. J. Jackson, and D. O. Scanlon, “sumo: Command-line tools for plotting and analysis of periodic ab initio calculations,” *Journal of Open Source Software* **28**, 717 (2018).
- ⁵⁴K. X. Steirer, P. Schulz, G. Teeter, V. Stevanovic, M. Yang, K. Zhu, and J. J. Berry, “Defect tolerance in methylammonium lead triiodide perovskite,” *ACS Energy Letters* **1**, 360–366 (2016), <https://doi.org/10.1021/acseenergylett.6b00196>.
- ⁵⁵J. Berry, T. Buonassisi, D. A. Egger, G. Hodes, L. Kronik, Y.-L. Loo, I. Lubomirsky, S. R. Marder, Y. Mastai, J. S. Miller, D. B. Mitzi, Y. Paz, A. M. Rappe, I. Riess, B. Rybtchinski, O. Stafsudd, V. Stevanovic, M. F. Toney, D. Zitoun, A. Kahn, D. Ginley, and D. Cahen, “Hybrid organic–inorganic perovskites (hoips): Opportunities and challenges,” *Advanced Materials* **27**, 5102–5112, <https://onlinelibrary.wiley.com/doi/pdf/10.1002/adma.201502294>.
- ⁵⁶P. S. Whitfield, N. Herron, W. E. Guise, K. Page, Y. Q. Cheng, I. Milas, and M. K. Crawford, “Structures, phase transitions and tricritical behavior of the hybrid perovskite methyl ammonium lead iodide,” *Scientific Reports* **6** (2016).
- ⁵⁷F. F. Targhi, Y. S. Jalili, and F. Kanjouri, “Mapbi3 and fapbi3 perovskites as solar cells: Case study on structural, electrical and optical properties,” *Results in Physics* **10**, 616 – 627 (2018).
- ⁵⁸R. Comin, G. Walters, E. S. Thibau, O. Voznyy, Z.-H. Lu, and E. H. Sargent, “Structural, optical, and electronic studies of wide-bandgap lead halide perovskites,” *J. Mater. Chem. C* **3**, 8839–8843 (2015).
- ⁵⁹F. Lehmann, A. Franz, D. M. TÅbbens, S. Levenco, T. Unold, A. Taubert, and S. Schorr, “The phase diagram of a mixed halide (br, i) hybrid perovskite obtained by synchrotron x-ray diffraction,” *RSC Adv.* **9**, 11151–11159 (2019).
- ⁶⁰L. Gil-Escrig, A. Miquel-Sempere, M. Sessolo, and H. J. Bolink, “Mixed iodide–bromide methylammonium lead perovskite-based diodes for light emission and photovoltaics,” *The Journal of Physical Chemistry Letters* **6**, 3743–3748 (2015), pMID: 26722750, <https://doi.org/10.1021/acs.jpcclett.5b01716>.
- ⁶¹G. Maculan, A. D. Sheikh, A. L. Abdelhady, M. I. Saidaminov, M. A. Haque, B. Murali, E. Alarousu, O. F. Mohammed, T. Wu, and O. M. Bakr, “Ch₃nh₃pbcI₃ single crystals: Inverse temperature crystallization and visible-blind uv-photodetector,” *The Journal of Physical Chemistry Letters* **6**, 3781–3786 (2015), pMID: 26722870, <https://doi.org/10.1021/acs.jpcclett.5b01666>.
- ⁶²S.-H. Wei, L. G. Ferreira, J. E. Bernard, and A. Zunger, “Electronic properties of random alloys: Special quasirandom structures,” *Phys. Rev. B* **42**, 9622–9649 (1990).
- ⁶³Z. Jiang, Y. Nahas, B. Xu, S. Prosandeev, D. Wang, and L. Bellaiche, “Special quasirandom structures for perovskite solid solutions,” *Journal of Physics: Condensed Matter* **28**, 475901 (2016).
- ⁶⁴J. Heyd, J. E. Peralta, G. E. Scuseria, and R. L. Martin, “Energy band gaps and lattice parameters evaluated with the heyd-scuseria-ernzerhof screened hybrid functional,” *The Journal of Chemical Physics* **123**, 174101 (2005), <https://doi.org/10.1063/1.2085170>.
- ⁶⁵F. Aryasetiawan and O. Gunnarsson, “TheGWmethod,” *Reports on Progress in Physics* **61**, 237–312 (1998).
- ⁶⁶R. Sun, M. K. Y. Chan, S. Kang, and G. Ceder, “Intrinsic stoichiometry and oxygen-induced *p*-type conductivity of pyrite feS₂,” *Phys. Rev. B* **84**, 035212 (2011).
- ⁶⁷E. M. Hutter, G. E. Eperon, S. D. Stranks, and T. J. Savenije, “Charge carriers in planar and meso-structured organic–inorganic perovskites: Mobilities, lifetimes, and concentrations of trap states,” *The Journal of Physical Chemistry Letters* **6**, 3082–3090 (2015), pMID: 26267206, <https://doi.org/10.1021/acs.jpcclett.5b01361>.
- ⁶⁸Q. Chen, H. Zhou, Y. Fang, A. Z. Stieg, T.-B. Song, H.-H. Wang, X. Xu, Y. Liu, S. Lu, J. You, P. Sun, J. McKay, M. S. Goorsky, and Y. Yang, “The optoelectronic role of chlorine in ch₃nh₃pbi₃(cl)-based perovskite solar cells,” *Nature Communications* **6**, 7269.
- ⁶⁹D. Kiermasch, P. Rieder, K. Tvingstedt, A. Baumann, and V. Dyakonov, “Improved charge carrier lifetime in planar perovskite solar cells by bromine doping,” *Scientific Reports* **6**, 39333.
- ⁷⁰Z. Chen, B. Turedi, A. Y. Alsalloum, C. Yang, X. Zheng, I. Gereige, A. AlSaggaf, O. F. Mohammed, and O. M. Bakr, “Single-crystal mapbi3 perovskite solar cells exceeding 21% power conversion efficiency,” *ACS Energy Letters* **4**, 1258–1259 (2019), <https://doi.org/10.1021/acseenergylett.9b00847>.
- ⁷¹Y. Bi, E. M. Hutter, Y. Fang, Q. Dong, J. Huang, and T. J. Savenije, “Charge carrier lifetimes exceeding 15 ns in methylammonium lead iodide single crystals,” *The Journal of Physical Chemistry Letters* **7**, 923–928 (2016), pMID: 26901658, <https://doi.org/10.1021/acs.jpcclett.6b00269>.
- ⁷²M. Anaya, G. Lozano, M. E. Calvo, and H. MÅguez, “Abx₃ perovskites for tandem solar cells,” *Joule* **1**, 769 – 793 (2017).
- ⁷³A. Sadhanala, S. Ahmad, B. Zhao, N. Giesbrecht, P. M. Pearce, F. Deschler, R. L. Z. Hoye, K. C. GÅdel, T. Bein, P. Docampo, S. E. Dutton, M. F. L. De Volder, and R. H. Friend, “Blue-green color tunable solution processable organolead chloride–bromide mixed halide perovskites for optoelectronic applications,” *Nano Letters* **15**, 6095–6101 (2015), pMID: 26236949, <https://doi.org/10.1021/acs.nanolett.5b02369>.
- ⁷⁴C. Li, X. Lu, W. Ding, L. Feng, Y. Gao, and Z. Guo, “Formability of ABX₃ (X = F, Cl, Br, I) halide perovskites,” *Acta Crystallographica Section B* **64**, 702–707 (2008).